Available online at www.eccomasproceedia.org
Eccomas Proceedia COMPDYN (2023) 1996-2008

ECCOMAS
Proceedia

COMPDYN 2023
9th ECCOMAS Thematic Conference on
Computational Methods in Structural Dynamics and Earthquake Engineering
M. Papadrakakis, M. Fragiadakis (eds.)
Athens, Greece, 12-14 June 2023

CLASSIFICATION AND PHENOMENOLOGICAL MODELING OF HYSTERESIS PHENOMENA IN ENERGY DISSIPATION DEVICES

Ciro Napolitano[1], Nicolò Vaiana[2], and Luciano Rosati [2]

[1]Department of Structures for Engineering and Architecture, University of Naples Federico II
Via Claudio 21, 80124 Napoli, Italy
e-mail: ciro.napolitano@unina.it

[2] Department of Structures for Engineering and Architecture, University of Naples Federico II
Via Claudio 21, 80124 Napoli, Italy
e-mail: {nicolo.vaiana,luciano.rosati}@unina.it

Abstract. *We present some preliminary results on the classification of rate-independent hysteretic loops exhibed by dampers. Furthermore, modellind of their hysteretic behavior is obtained by means of a recently formulated phenomenological model that allows for a closed-form evaluation of the nonlinear force-displacement, or their generalized counterparts, relationship and of the associated dissipated energy.*

After a brief presentation of the essential feartures of the model, the proposed approach is applied to reproduce the experimenatl behaviour of two dissipation devices.

Keywords: Classification Dampers, Energy Dissipation Device, Hysteretic Behavior, Phenomenological Model, Internal Energy Change.

ISSN:2623-3347
Peer-review under responsibility of the organizing committee of COMPDYN 2023.
doi: 10.7712/120123.10537.20626

1 INTRODUCTION

Damping systems represent one of the most effective techniques for the seismic protection of buildings [1] together with seismic isolation [2] [3] [4] [5] [6]. The need to introduce these seismic protection techniques derives from the economic impossibility of creating structures resistant to any earthquake [7]. Hence, damper systems are designed and manufactured to protect structural integrities, control structural damages, and to prevent injuries to the residents by absorbing seismic energy and reducing deformations in the structure [10]. Specifically, seismic dampers permit the structure to resist severe input energy and reduce harmful deflections, forces and accelerations to structures and occupants.

Dampers, that are effective not only against earthquakes but also against wind induced vibrations, are inserted in the full height structures so as to diffuse in the structural elements [15] the energy transferred from external actions, mainly of authropic nature.

In spite of the significant technological advancements in the design of passive dampers, their effective positioning within the structure and, above all, the exact evaluation of the amount of energy they can actually dissipate still represents an active topic of research. Within the large class of seismic dampers, namely viscous , friction , yielding, magnetic and tuned mass damper, see, e.g., Soong TT and BFJr (2002) [8] and Symans MD et al (2008) [9] for a survey account, we are interested to those having a rate-independent hysteretic behavior [14], i.e. devices in which the restoring force is function of the displacement.

In particular, we shall make reference to two separate examples of *metallic* and *friction dampers* [13] to illustrate the application of the brend-new hysteretic model by Vaiana and Rosati (2023) [15] able to supply for a general classification of rate-independent hysteretic behaviour and allow for an analytical evaluation of hysteretic loops by means of two sets of eight parameters [15].

In the first part of this paper (Section 2) we briefly illustrate the Vaiana-Rosati Model (VMR), which offers a number of advantages compared to other hysteretic models available in the literature. In the second part of this paper (Section 3) we show how to calculate the energy dissipated by hysteretic loops according to the approach presented in [16].

Finally, in the third part (Section 4), the experimental hysteretic loopsof two devices, namely Steel Self-Centering Device [17] and Slit Damper Systems [18], are modelled using the VRM and the dissipated energy of the hysteretic loops is computed.

2 VAIANA-ROSATI MODEL

Let us first summarise the basic elements of the Vaiana-Rosati model proposed in [15] to characterize the rate-independent hysteretic behaviours of mechanical systems and materials in which a generalered force f is related to a generalized dispacement u [11] [12].

The model classifies hysteresis loops into four main categories namely loops limited: (i) by two straight lines (shape type $S1$), (ii) by two curves with no inflection point (shape type $S2$), by two curves with one inflection point (shape type $S3$), by two curves with two inflection points (shape type $S4$). All hysteresis loops are shown in Figure 1 and are further commented in the sequel since each category, or class, can be specialized to several subclasses.

To be specific, the $S1$ class include three separate shape types ($S1a$, $S1b$, $S1c$), all having an asymmetric shape; indeed, the limiting straight lines in the $S1a$ shape type are not parallel, while in the $S1b$ shape type the upper and lower straight lines are not symmetric about the horizontal axis; finally in the $S1c$ shape type the generic loading and unloading curves are not symmetric about the origin.

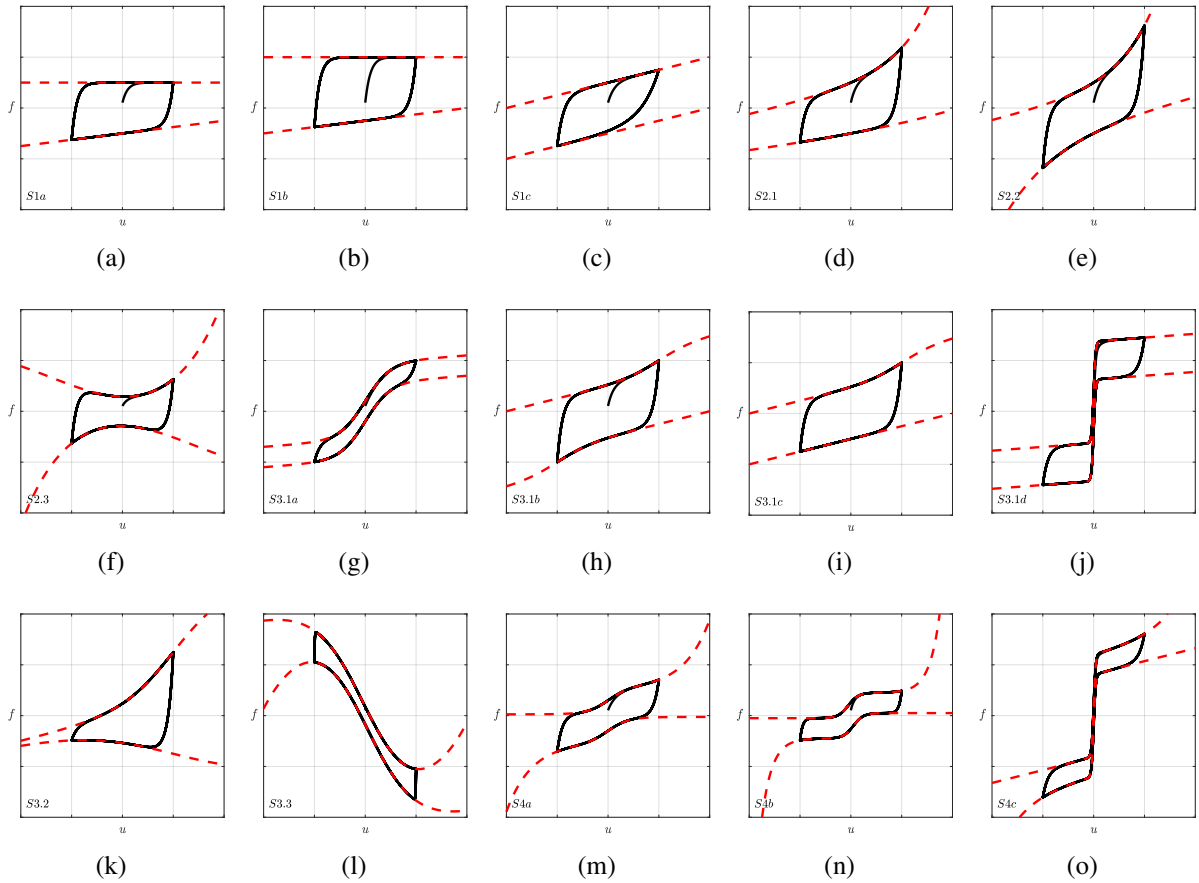

Figure 1: Classification of hysteresis loops.

Analogously, hysteresis loops of the $S2$ type include three different subclasses depending on the analytical properties of the bounding curves, all having no inflection point as common feature. Actually, in the first one the two bounds are convex limiting curves; in the second one the upper (lower) bound is a convex (concave) limiting curve having no absolute minimum (maximum) value, whereas, in the third one the upper (lower) bound is a convex (concave) limiting curve that has an absolute minimum (maximum) value.

The six hysteresis loops of type $S3$ ($S3.1a$, $S3.1b$, $S3.1c$, $S3.1d$, $S3.2$, and $S3.3$) are all limited by two curves with one inflection point but it is possible to identify three shape subtypes ($S3.1$, $S3.2$, and $S3.3$). Moreover, we can further subdivide the $S3.1$ tipology into four hysteresis loops ($S3.1a$, $S3.1b$, $S3.1c$, $S3.1d$) that are bounded by two increasing S-shaped limiting curves, while the subtype $S3.2$ is limited by an upper increasing (a lower decreasing) S-shaped limiting curve, whereas the subtype $S3.3$ is limited by two decreasing S-shaped limiting curves.

The hysteresis loops of type $S4$ are bounded by two curves having two inflection points and display three different shape types ($S4a$, $S4b$, and $S4c$), the first and second ones being pinched, whereas the third one is flag-shaped.

Figure 2 shows the essential elements used to model a generic hysteretic loop, namely an arbitrary loading curve, an upper limit curve, a generic unloading curve, a lower limit curve and the internal variables u_j^+ (u_j^-).

In particular, the Vaiana-Rosati model: (i) allows for the evaluation of the generalized force in closed form thus requiring a reduced computational effort, (ii) is capable of reproducing all the different types of complex hysteresis loops previously illustrated, (iii) is based on param-

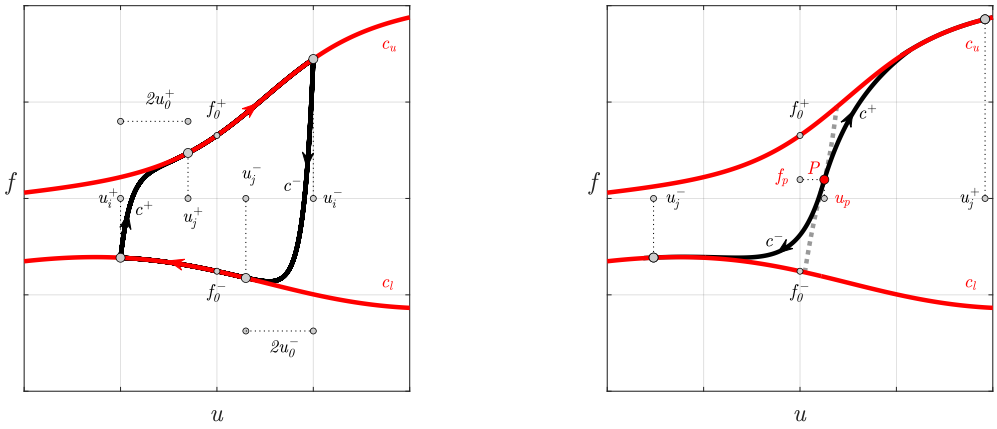

(a) (b)

Figure 2: (a) VRM formulation: curves c^+ (loading), c^- (unloading), c_u (upper), c_l (lower); (b) internal variables u_j^+ and u_j^- associated with a generic hysteresis loop.

eters that allow one to manage the loading (unloading) phase independently of the unloading (loading) one, (iv) adopts parameters describing specific theoretical and/or experimental properties of the hysteresis loops, thus simplifying the identification procedure, and (v) can be easily implemented in a computer program.

The eight parameters to be used for the generic load curve (unloading) are the following: k_b^+, f_0^+, α^+, β_1^+, β_2^+, γ_1^+, γ_2^+, γ_3^+ (k_b^-, f_0^-, α^-, β_1^-, β_2^-, γ_1^-, γ_2^-, γ_3^-); they are required to satisfy the following conditions: $f_0^+ > 0$, $\alpha^+ > 0$ ($f_0^- > 0$, $\alpha^- > 0$), whereas k_b^+, β_1^+, β_2^+, γ_1^+, γ_2^+, γ_3^+ (k_b^-, β_1^-, β_2^-, γ_1^-, γ_2^-, γ_3^-) can be arbitrary real numbers. In the case of the generic loading (unloading) curve the sign of the generalized velocity $\dot{u}$ is positive (negative).

During the generic loading phase ($\dot{u} > 0$), the generalized force f is given by:

$$f(u,u_j^+) = \begin{cases} c^+(u,u_j^+) & \text{when} \quad u < u_j^+ \quad (1a) \\ c_u(u) & \text{when} \quad u > u_j^+, \quad (1b) \end{cases}$$

while, during the generic unloading phase ($\dot{u} < 0$), it is represented by the following expression:

$$f(u,u_j^-) = \begin{cases} c^-(u,u_j^-) & \text{when} \quad u > u_j^- \quad (2a) \\ c_l(u) & \text{when} \quad u < u_j^-. \quad (2b) \end{cases}$$

in which c^+ and c^- represent, respectively, the generic loading and unloading curve. Their expressions, reported in [15], are:

$$\begin{aligned} c^+(u,u_j^+) = &\beta_1^+ e^{\beta_2^+ u} - \beta_1^+ + \frac{4\gamma_1^+}{1+e^{-\gamma_2^+(u-\gamma_3^+)}} - 2\gamma_1^+ + k_b^+ u + \\ &+ f_0^+ - \frac{1}{\alpha^+}\left[e^{-\alpha^+\left(+u-u_j^+ + \bar{u}^+\right)} - e^{-\alpha^+ \bar{u}^+}\right], \end{aligned} \quad (3)$$

$$\begin{aligned} c^-(u,u_j^-) =& \beta_1^- e^{\beta_2^- u} - \beta_1^- + \frac{4\gamma_1^-}{1+e^{-\gamma_2^-\left(u-\gamma_3^-\right)}} - 2\gamma_1^- + k_b^- u + \\ & - f_0^- + \frac{1}{\alpha^-}\left[e^{-\alpha^-\left(-u+u_j^-+\bar{u}^-\right)} - e^{-\alpha^-\bar{u}^-}\right], \end{aligned} \tag{4}$$

while c_u and c_l are, respectively, the upper and lower limit curve:

$$c_u(u) = \beta_1^+ e^{\beta_2^+ u} - \beta_1^+ + \frac{4\gamma_1^+}{1+e^{-\gamma_2^+\left(u-\gamma_3^+\right)}} - 2\gamma_1^+ + k_b^+ u + f_0^+, \tag{5}$$

$$c_l(u) = \beta_1^- e^{\beta_2^- u} - \beta_1^- + \frac{4\gamma_1^-}{1+e^{-\gamma_2^-\left(u-\gamma_3^-\right)}} - 2\gamma_1^- + k_b^- u - f_0^-. \tag{6}$$

The generic loading curve c^+ intersects the lower (upper) limit curve at a generic point having abscissa u_i^+ (u_j^+) with $u_i^+ = u_j^+ - 2u_0^+$, and the upper limit curve c_u intercepts the vertical axis at $f = f_0^+$; similarly, the generic unloading curve c^- intersects the upper (lower) limiting curve at a generic point having abscissa u_i^- (u_j^-), with $u_i^- = u_j^- - 2u_0^-$, and the lower limiting curve c_l intercepts the vertical axis at $f = -f_0^-$.

The internal variable u_j^+ (u_j^-), associated with the generic loading (unloading) phase, is given by the following expression:

$$\begin{aligned} u_j^+ =& u_P + \bar{u}^+ + \frac{1}{\alpha^+}\ln\Bigg\{ + \alpha^+\Bigg[\beta_1^+ e^{\beta_2^+ u_P} - \beta_1^+ + \frac{4\gamma_1^+}{1+e^{-\gamma_2^+\left(u_P-\gamma_3^+\right)}} \\ & - 2\gamma_1^+ + k_b^+ u_P + f_0^+ + \frac{1}{\alpha^+}e^{-\alpha^+\bar{u}^+} - f_P\Bigg]\Bigg\}, \end{aligned} \tag{7}$$

$$\begin{aligned} u_j^- =& u_P - \bar{u}^- - \frac{1}{\alpha^-}\ln\Bigg\{ - \alpha^-\Bigg[\beta_1^- e^{\beta_2^- u_P} - \beta_1^- + \frac{4\gamma_1^-}{1+e^{-\gamma_2^-\left(u_P-\gamma_3^-\right)}} \\ & - 2\gamma_1^- + k_b^- u_P - f_0^- - \frac{1}{\alpha^-}e^{-\alpha^-\bar{u}^-} - f_P\Bigg]\Bigg\}, \end{aligned} \tag{8}$$

where u_p and f_P are the coordinates of the initial point of c^+ (c^-); while, $\bar{u}^+$ ($\bar{u}^-$) are parameters internal to the model defined by the following expression:

$$\bar{u}^+ = -\frac{1}{\alpha^+}\ln\left(\delta_k^+\right), \tag{9}$$

$$\bar{u}^- = -\frac{1}{\alpha^-}\ln\left(\delta_k^-\right), \tag{10}$$

with δ_k^+ (δ_k^-) to be set equal to 10^{-20}.

For more information the reader is referred to the original article [15].

3 INTERNAL ENERGY

In this section, we derive the expressions to evaluate the path-dependent work done by generalized non-conservative internal forces and the change in internal energy associated with path-dependent work (dissipated energy).

Figures 3 and 4 show the four contributions (W^+, W_u, W^-, W_l) that allow us to calculate the *rate-independent* hysteretic work W_{ri} of a cycle simulated using the Vaiana Rosati model, in which W^+ (W_u) represents the area under the curve c^+ (c_u) over $[u_i, u_f]$, whereas W^- (W_l) represents the area under the curve c^- (c_l) over $[u_f, u_i]$.

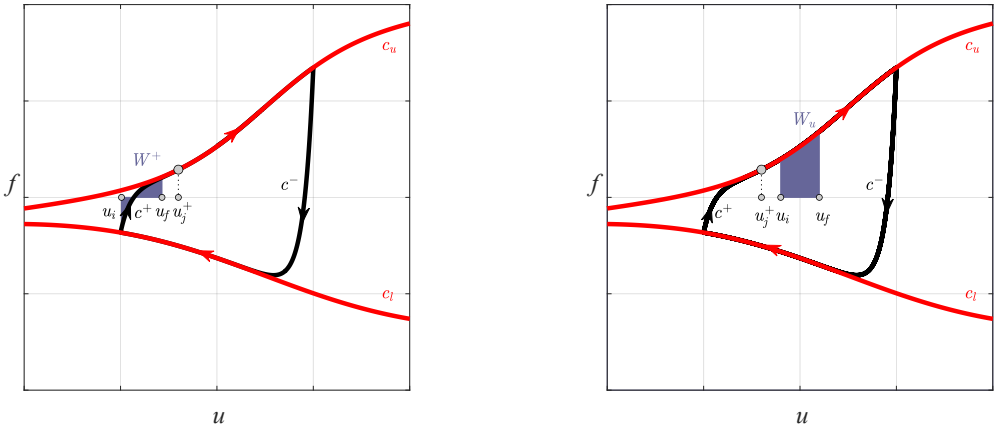

Figure 3: Evaluation of the rate-independent work during a generic loading phase when: $u < u_j^+$ (a) and $u > u_j^+$ (b).

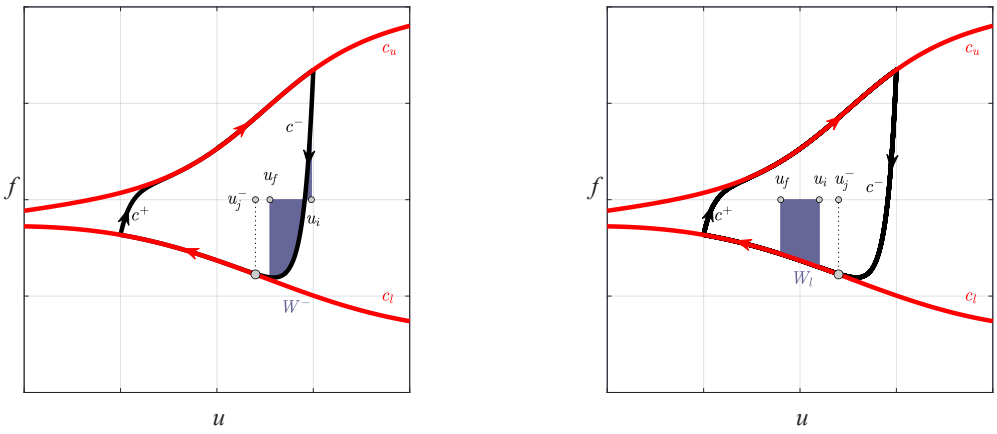

Figure 4: Evaluation of the rate-independent work during a generic unloading phase when: $u > u_j^-$ (a) and $u < u_j^-$ (b).

In particular, during a generic loading phase ($\dot{u} > 0$), the *rate-independent* hysteretic work W_{ri} is evaluated as:

$$W_{ri} = \begin{cases} W^+ & \text{when} \quad u < u_j^+ \quad (11a) \\ W_u & \text{when} \quad u > u_j^+, \quad (11b) \end{cases}$$

whereas, during a generic unloading phase ($\dot{u} < 0$), the *rate-independent* hysteretic work W_{ri} is evaluated as:

$$W_{ri} = \begin{cases} W^- & \text{when} \quad u > u_j^- \quad (12a) \\ W_l & \text{when} \quad u < u_j^-, \quad (12b) \end{cases}$$

To obtain the closed-form expression of W^+ (W_u) it is convenient to write the generic load curve c^+ (the upper limit curve c_u) as follows:

$$c^+(u, u_j^+) = c_a^+(u) + c_b^+(u) + c_c^+(u) + c_d^+(u, u_j^+), \quad (13)$$

$$c_u(u) = c_a^+(u) + c_b^+(u) + c_c^+(u), \quad (14)$$

whereas, to obtain the closed-form expression of W^- (W_l) it is useful to write the generic load curve c^- (the upper limit curve c_l) as follows:

$$c^-(u, u_j^-) = c_a^-(u) + c_b^-(u) + c_c^-(u) + c_d^-(u, u_j^-), \quad (15)$$

$$c_l(u) = c_a^-(u) + c_b^-(u) + c_c^-(u), \quad (16)$$

with c_a^+, c_b^+, c_c^+, c_d^+ defined as:

$$c_a^+(u) = \beta_1^+ e^{\beta_2^+ u} - \beta_1^+, \quad (17a)$$

$$c_b^+(u) = \frac{4\gamma_1^+}{1 + e^{-\gamma_2^+ (u - \gamma_3^+)}} - 2\gamma_1^+, \quad (17b)$$

$$c_c^+(u) = k_b^+ u + f_0^+, \quad (17c)$$

$$c_d^+(u, u_j^+) = -\frac{1}{\alpha^+} \left[e^{-\alpha^+ (+u - u_j^+ + \bar{u}^+)} - e^{-\alpha^+ \bar{u}^+} \right], \quad (17d)$$

and c_a^-, c_b^-, c_c^-, c_d^- given by:

$$c_a^-(u) = \beta_1^- e^{\beta_2^- u} - \beta_1^-, \quad (18a)$$

$$c_b^-(u) = \frac{4\gamma_1^-}{1 + e^{-\gamma_2^- (u - \gamma_3^-)}} - 2\gamma_1^-, \quad (18b)$$

$$c_c^-(u) = k_b^- u - f_0^-, \quad (18c)$$

$$c_d^-(u, u_j^-) = +\frac{1}{\alpha^-} \left[e^{-\alpha^- (-u + u_j^- + \bar{u}^-)} - e^{-\alpha^- \bar{u}^-} \right]. \quad (18d)$$

The expression of W^+ (W_u) can be obtained by integrating Equation (13) ((14)) over $[u_i, u_f]$:

$$W^+ = \int_{u_i}^{u_f} c^+(u, u_j^+) \, \mathrm{d}u = \int_{u_i}^{u_f} \left(c_a^+ + c_b^+ + c_c^+ + c_d^+ \right) \mathrm{d}u = W_a^+ + W_b^+ + W_c^+ + W_d^+, \quad (19)$$

$$W_u = \int_{u_i}^{u_f} c_u(u)\,\mathrm{d}u = \int_{u_i}^{u_f} \left(c_a^+ + c_b^+ + c_c^+\right)\,\mathrm{d}u = W_a^+ + W_b^+ + W_c^+. \tag{20}$$

whereas the expression of W^- (W_l) can be obtained by integrating Equation (15) ((16)) over $[u_f, u_i]$:

$$W^- = \int_{u_i}^{u_f} c^-(u, u_j^-)\,\mathrm{d}u = \int_{u_i}^{u_f} \left(c_a^- + c_b^- + c_c^- + c_d^-\right)\,\mathrm{d}u = W_a^- + W_b^- + W_c^- + W_d^-, \tag{21}$$

$$W_l = \int_{u_i}^{u_f} c_l(u)\,\mathrm{d}u = \int_{u_i}^{u_f} \left(c_a^- + c_b^- + c_c^-\right)\,\mathrm{d}u = W_a^- + W_b^- + W_c^-. \tag{22}$$

In particular W_a^+, W_b^+, W_c^+, W_d^+, are computed as:

$$W_a^+ = \frac{\beta_1^+}{\beta_2^+}\left(e^{\beta_2^+ u_f} - e^{\beta_2^+ u_i}\right) - \beta_1^+(u_f - u_i), \tag{23a}$$

$$W_b^+ = 2\gamma_1^+\left\{\frac{2\ln\left[e^{-\gamma_2^+(u_f-\gamma_3^+)}+1\right]}{\gamma_2^+} - \frac{2\ln\left[e^{-\gamma_2^+(u_i-\gamma_3^+)}+1\right]}{\gamma_2^+} + (u_f - u_i)\right\}, \tag{23b}$$

$$W_c^+ = \frac{k_b^+}{2}(u_f^2 - u_i^2) + f_0^+(u_f - u_i), \tag{23c}$$

$$W_d^+ = +\frac{1}{(\alpha^+)^2}\,e^{-\alpha^+(\bar{u}^+ - u_j^+)}\left[\alpha^+(u_f - u_i)e^{-\alpha^+ u_j^+} + e^{-\alpha^+ u_f} - e^{-\alpha^+ u_i}\right]. \tag{23d}$$

while W_a^-, W_b^-, W_c^-, W_d^- are given by:

$$W_a^- = \frac{\beta_1^-}{\beta_2^-}\left(e^{\beta_2^- u_f} - e^{\beta_2^- u_i}\right) - \beta_1^-(u_f - u_i), \tag{24a}$$

$$W_b^- = 2\gamma_1^-\left\{\frac{2\ln\left[e^{-\gamma_2^-(u_f-\gamma_3^-)}+1\right]}{\gamma_2^-} - \frac{2\ln\left[e^{-\gamma_2^-(u_i-\gamma_3^-)}+1\right]}{\gamma_2^-} + (u_f - u_i)\right\}, \tag{24b}$$

$$W_c^- = \frac{k_b^-}{2}(u_f^2 - u_i^2) - f_0^-(u_f - u_i), \tag{24c}$$

$$W_d^- = -\frac{1}{(\alpha^-)^2}\,e^{-\alpha^-(\bar{u}^- + u_j^-)}\left[\alpha^-(u_f - u_i)e^{+\alpha^- u_j^-} - e^{+\alpha^- u_f} + e^{+\alpha^- u_i}\right]. \tag{24d}$$

The closed form expression of such an internal energy change $\Delta(E_I)_{ri}$ can be obtained adding the four contributions calculated previously(19, 20, 21, 22):

$$\Delta(E_I)_{ri} = +\int_{u_i^+}^{u_j^+} c^+(u, u_j^+)\,\mathrm{d}u + \int_{u_j^+}^{u_i^-} c_u(u)\,\mathrm{d}u + \int_{u_i^-}^{u_j^-} c^-(u, u_j^-)\,\mathrm{d}u + \int_{u_j^-}^{u_i^+} c_l(u)\,\mathrm{d}u, \tag{25}$$

where u_i^+ (u_i^-) represents the abscissa of the intersection point of c^+ (c^-) and c_l (c_u), whereas u_j^+ (u_j^-) is the abscissa of the intersection point of c^+ (c^-) and c_u (c_l).

Substituting the formulas (13)-(16), in the equation (25), one has:

$$\Delta(E_I)_{ri} = + \int_{u_i^+}^{u_i^-} (c_a^+ + c_b^+ + c_c^+)\,\mathrm{d}u + \int_{u_i^+}^{u_j^+} c_d^+\,\mathrm{d}u + \int_{u_i^-}^{u_i^+} (c_a^- + c_b^- + c_c^-)\,\mathrm{d}u + \int_{u_i^-}^{u_j^-} c_d^-\,\mathrm{d}u, \quad (26)$$

$$\Delta(E_I)_{ri} = +W_a^+ + W_b^+ + W_c^+ + W_d^+ + W_a^- + W_b^- + W_c^- + W_d^-; \quad (27)$$

more information can be found in [16].

4 NUMERICAL APPLICATIONS

The main aim of this section is to show the capability of the presented model to simulate very different types of complex hysteresis phenomena that characterize the experimental response of specific dampers when they are subjected to a cyclic generalized displacement history having different amplitudes. In particular, this operation is performed with reference to the hysteresis loops obtained during some experimental tests conducted on Steel Self-Centering Device (SSCD) [17] and Slit Damper Systems [18].

The SSCD studied by Bracconi et al.[17], is made up of three groups of elements, each one having speci ɔn Elements, see, e.g., Fig

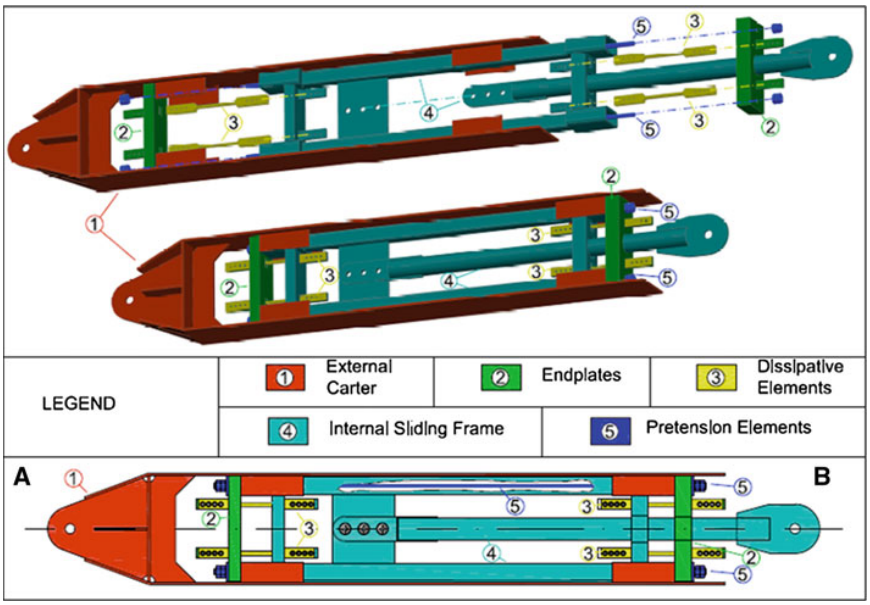

Figure 5: Steel Self-Centering Device (SSCD) illustrated in [17].

The Skeleton serves to transmit and distribute external forces between the Dissipative Elements and the Pretension Elements. The Dissipative Elements, located within the skeleton, are made up of dog bone shaped steel elements and represent the part where energy is dissipated. The Pretension Elements, made of prestressing cables, are located within the Skeleton and connect both extremities of the SSCD to the structural frames. The elements are positioned and connected to each other in order to ensure the same global behavior of the SSCD device under both tension and compression external forces.

Figure 6a illustrates the comparison between the experimental hysteresis loops and those predicted by the proposed model (VRM, Section 2) using the parameters listed in Table 1.

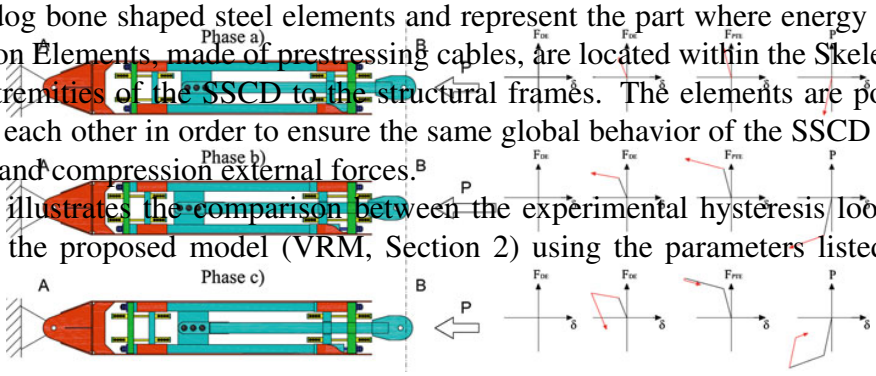

Fig. 3 Main phases of SSCD behavior under external compression force

According to the classification illustrated in Figure 1, the hysteresis loop of the SSCD belongs to the $S3.1d$ class since it is limited by two curves with one inflection point; specifically the experimental hysteresis loops are bounded by two increasing S-shaped limiting curves (flag-shaped symmetric). Moreover, using the path of reasoning detailed in Section 3, we report in Figure 6b the internal energy dissipated by the wider hysteresis loop presented in Figure 6a.

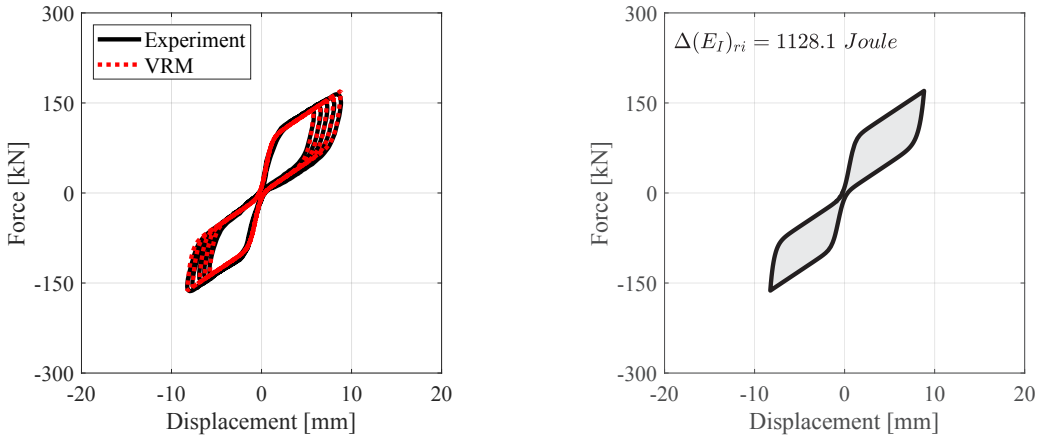

(a) (b)

Figure 6: (a) Experimental hysteresis loop in Bracconi et al [17] versus simulated ones; (b) values of the dissipated energy for the wider hysteresis loop.

sign $\dot{u}$	k_b $[Nm^{-1}]$	α $[m^{-1}]$	f_0 $[N]$	β_1 $[N]$	β_2 $[m^{-1}]$	γ_1 $[N]$	γ_2 $[m^{-1}]$	γ_3 $[m]$
+	10	2.5	38	-0.1	0.1	22	3.0	0.5
-	10	2.0	40	0.1	0.1	20	3.0	-0.7

Table 1: Parameters used to reproduce the hysteretic responses in Figures 6.

The Slit Damper Systems, studied by Seo et al [18] and illustrated in Figure 7, have been designed to be incorporated into the bracing system of structural frames; these dampers are installed on the top of shaped V braces at the concentrically braced frames, and attached to the middle of the horizontal beam.

Slit dampers are manufactured from standard wide flange sections with a number of slits cut from the web, thereby leaving a number of strips between the two flanges and producing the part where energy is dissipated. The slits are rounded at their ends with the aim of avoiding stress concentration in the reentrant corners. Slit dampers are connected to the main frame member with four bolts.

Figures 8a illustrates the comparison between the experimental hysteresis loops and those predicted by using the proposed model (VRM, Section 2) with the parameters listed in Table 2. In this case the hysteresis loops are bounded by two increasing limiting curve so that they can be classified as $S3.1a$ according to the notation introduced in Figure 1. The internal energy dissipated by the wider hysteresis loop of the Slit Damper Systems, obtained as shown in Section 3, is provided in Figure 8b.

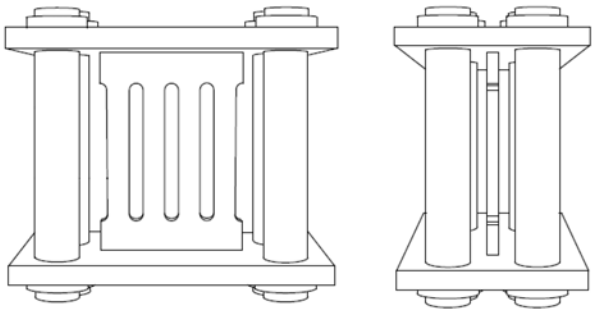

Figure 7: Slit Damper Systems illustrated in [18].

Figure 5. Design of the slit damper system with recentering SMA bars (**a**): Front View;

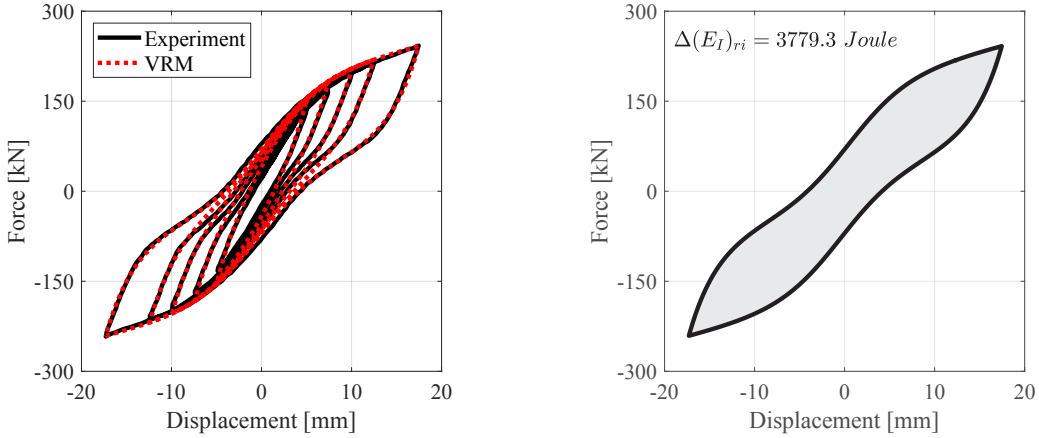

simulated by superposing superelastic SMA behavior and energy dissipation behavior. As can be seen in Figure 6, these component behaviors are assembled in parallel depending on how they interact each other. Owing to such parallel assemblage, the total force of the recentering slit damper system (P) can be determined by adding together component forces under the corresponding displacement (Δ) as follows:

Figure 8: (a) Experimental hysteresis loop in Seo et al [18] versus simulated ones; (b) values of the dissipated energy for the wider hysteresis loop.

$$P = P_{SMA} + P_{slit} \tag{1}$$

sign $\dot{u}$	k_b $[Nm^{-1}]$	α $[m^{-1}]$	f_0 $[N]$	β_1 $[N]$	β_2 $[m^{-1}]$	γ_1 $[N]$	γ_2 $[m^{-1}]$	γ_3 $[m]$
+	3.7	0.32	78	0.1	0.1	50	0.3	0.5
-	3.7	0.32	78	0.1	0.1	50	0.3	-0.5

Table 2: Parameters used to reproduce the hysteretic responses in Figures 8.

5 CONCLUSIONS

We have presented a preliminary analysis of the hysteresis loops exhibited by dampers, based on the application of the brand-new Vaiana-Rosati model, to be further developed in a future article. The great advantage of using the Vaiana-Rosati model lies in its accuracy in reproducing the hysteretic behavior of several mechanical systems and materials as well a in the large number of different hysteretic loops that can be simulated.

Due to space limitations the model has been applied only to two dampers; however it has been given a general overview of how the Vaiana-Rosati model classifies hysteresis loops and computes the associated dissipated energy.

Actually, a classification of the hysteresis loops is important because it allows the reader to

have an idea about the different types of hysteresis loops, referred to dampers, that exist in the literature.

Finally, the amount of energy dissipated by each specific damper is a very important information in the design of these elements since it allows one to evaluate how much energy can be dissipated without causing major damage to the structure.

REFERENCES

[1] T.T. Soong, G.F. Dargush, Passive energy dissipation systems in structural engineering, *Wiley*, 1997.

[2] F. Cilento, D. Losanno, L. Piga, An experimental study on a novel reclaimed rubber compound for fiber-reinforced seismic isolators, *Structures*, **45**, 9-22, 2022.

[3] D. Losanno, D. De Domenico, I.E. Madera-Sierra, Experimental testing of full-scale fiber reinforced elastomeric isolators (FREIs) in unbounded configuration, *Engineering Structures*, **260**, 114234, 2022.

[4] A. Orfeo, E. Tubaldi, A. H. Muhr, D. Losanno, Mechanical behaviour of rubber bearings with low shape factor, *Engineering Structures*, **266**, 114532, 2022.

[5] D. Pellecchia, N. Vaiana, M. Spizzuoco, G. Serino, L. Rosati, Axial hysteretic behaviour of wire rope isolators: Experiments and modelling, *Materials & Design*, **225**, 111436, 2023.

[6] D. De Domenico, D. Losanno, N. Vaiana, Experimental tests and numerical modeling of full-scale unbonded fiber reinforced elastomeric isolators (UFREIs) under bidirectional excitation, *Engineering Structures*, **274**, 115118, 2023.

[7] I.D. Aiken, J.M. Kelly, Comparative study of four passive energy dissipation systems, *Bulletin of the New Zealand National Society for Earthquake Engineering*, **25**(3), 175–192, 1992.

[8] T.T. Soong, B.F. Jr Spencer, Supplemental energy dissipation: state-of-the-art and stateofthepractice, *Eng Struct*, **24**(3), 243–259, 2002.

[9] M. D. Symans, F. A. Charney, A. S. Whittaker, M. C. Constantinou, Energy dissipation systems for seismic applications: current practice and recent developments. *J Struct Eng ASCE*, **134**(1), 3–21, 2008.

[10] N. Vaiana, C. Napolitano, L. Rosati, Some recent advances on the modeling of the hysteretic behavior of rate-independent passive energy dissipation devices, *Proceedings of COMPDYN 2021*, 2435-2445, 2021.

[11] N. Vaiana, S. Sessa, F. Marmo, L. Rosati, A class of uniaxial phenomenological models for simulating hysteretic phenomena in rate-independent mechanical systems and materials. *Nonlinear Dynamics*, **93**(3), 1647-1669, 2018.

[12] N. Vaiana, S. Sessa, L. Rosati, A generalized class of uniaxial rate-independent models for simulating asymmetric mechanical hysteresis phenomena, *Mechanical Systems and Signal Processing*, **146**, 106984, 2021.

[13] N. Vaiana, S. Sessa, F. Marmo, L. Rosati, An accurate and computationally efficient uniaxia phenomenological model for steel and fiber reinforced elastomeric bearings, *Composite Structures*, **211**, 196-212, 2019.

[14] N. Vaiana, D. Losanno, N. Ravichandran, A novel family of multiple springs models suitable for biaxial rate-independent hysteretic behavior, *Computers & Structures*, **244**, 106403, 2021.

[15] N. Vaiana, L. Rosati, Classification and unified phenomenological modeling of complex uniaxial rate-independent hysteretic responses, *Mechanical Systems and Signal Processing*, **182**, 109539, 2023.

[16] N. Vaiana, R. Capuano, L. Rosati, Evaluation of path-dependent work and internal energy change for hysteretic mechanical systems, *Mechanical Systems and Signal Processing*, **186**, 109862, 2023.

[17] A. Braconi, F. Morelli, W. Salvatore, Development, design and experimental validation of a steel self-centering device (SSCD) for seismic protection of buildings. *Bull Earthquake Eng*, **10**, 1915–1941, 2012.

[18] J. Seo, Y.C. Kim, Hu, J.W. Pilot Study for Investigating the Cyclic Behavior of Slit Damper Systems with Recentering Shape Memory Alloy (SMA) Bending Bars Used for Seismic Restrainers, *Applied Sciences*, **5**, 187-208, 2015.